Biosensors and Bioelectronics 75 (2016) 88–95

Contents lists available at ScienceDirect

Biosensors and Bioelectronics

journal homepage: www.elsevier.com/locate/bios

Nanoplasmonic biochips for rapid label-free detection of imidacloprid pesticides with a smartphone

Kuang-Li Lee [a], Meng-Lin You [b], Chia-Hsin Tsai [c], En-Hung Lin [a], Shu-Yi Hsieh [a], Ming-Hsun Ho [d], Ju-Chun Hsu [c,*], Pei-Kuen Wei [a,b,e,**]

[a] Research Center for Applied Sciences, Academia Sinica, Taipei 11529, Taiwan
[b] Institute of Biophotonics, National Yang-Ming University, Taipei 11221, Taiwan
[c] Department of Entomology, National Taiwan University, Taipei 10617, Taiwan
[d] Agricultural Chemicals And Toxic Substances Research Institute, Taichung 41358, Taiwan
[e] Department of Optoelectronics, National Taiwan Ocean University, Keelung 20224, Taiwan

ARTICLE INFO

Article history:
Received 5 May 2015
Received in revised form
4 August 2015
Accepted 8 August 2015
Available online 10 August 2015

Keywords:
Optical biosensor
Nanostructure
Surface plasmon resonance
Spectral image
Imidacloprid insecticide
Label-free detection

ABSTRACT

The widespread and intensive use of neonicotinoid insecticides induces negative cascading effects on ecosystems. It is desirable to develop a portable sensitive sensing platform for on-site screening of high-risk pesticides. We combined an indirect competitive immunoassay, highly sensitive surface plasmon resonance (SPR) biochip and a simple portable imaging setup for label-free detection of imidacloprid pesticides. The SPR biochip consists of several capped nanoslit arrays with different periods which form a spectral image on the chip. The qualitative and semiquantitative analyses of pesticides can be directly observed from the spot shift on the chip. The precise semiquantitative analyses can be further completed by using image processing in a smartphone. We demonstrate simultaneous detection of four different concentrations of imidacloprid pesticides. The visual detection limit is about 1 ppb, which is well below the maximum residue concentration permitted by law (20 ppb). Compared to the one-step strip assay, the proposed chip is capable of performing semiquantitative analyses and multiple detection. Compared to the enzyme-linked immunosorbent assay, our method is label-free and requires simple washing steps and short reaction time. In addition, the label-free chip has a comparable sensitivity but wider working range than those labeling techniques.

1. Introduction

To increase the efficiency of farming, a family of compounds called neonicotinoids for soil injection, seed treatments and foliar spray is commonly used. Recent studies have shown that widespread and intensive use of neonicotinoid insecticides has been linked to declining honey bee and bird populations and negative cascading effects on ecosystems (Henry et al., 2012; Whitehorn et al., 2012; Hallmann et al., 2014; Goulson, 2013; Van der Sluijs et al., 2015). Imidacloprid is the most widespread insecticide among the neonicotinoids. It kills insects by binding nicotinic acetylcholine receptors (nAChR) in the central nervous system of insects. Imidacloprid is highly specific for the nAChR found in insects and less harmful to mammals. However, it is soluble in water and has a long lifetime greater than 1000 days, which make it accumulate in soils or run off into water sources and ultimate spread through the environment. Therefore, an effective and quick detection of such high-risk pesticide is important to prevent potential negative effects on ecosystems. For efficient pesticide identification and quantification, standard analytical methods such as high performance liquid chromatography (HPLC), gas chromatography (GC) and liquid chromatography (LC) combined mass spectrometry (MS) are commonly used. Although being sensitive and specific, these methods are high cost, time-consuming sample-preparation procedures and need highly trained technical personnel. In order to fulfill the requirement of rapid, simple, selective and sensitive detection, enzyme-linked immunosorbent assays (ELISAs) have been developed for detection of neonicotinoids in different matrices (Li and Li, 2000; Kim et al., 2004, 2006; Watanabe et al., 2004, 2013; Fang et al., 2011; Wang et al., 2012). However, repeated washing steps make the ELISA method difficult for one-step multiple assays. In contrast to the

* Corresponding author.
** Corresponding author at: Research Center for Applied Sciences, Academia Sinica, Taipei 11529, Taiwan.
E-mail addresses: juchun@ntu.edu.tw (J.-C. Hsu), pkwei@sinica.edu.tw (P.-K. Wei).

http://dx.doi.org/10.1016/j.bios.2015.08.010
0956-5663/

ELISA method, an immune-chromatographic assay or lateral-flow assay using colloidal gold as the label requires an assay procedure of only one step (Posthuma-Trumpie et al., 2009). It is portable, easy and convenient to use without specialized laboratory equipment. Such a strip assay has been utilized for qualitative detection of imidacloprid through naked eyes (Xu et al., 2012). Different from the previous techniques requiring the assistance of labels, surface plasmon resonance (SPR) sensing is a real-time and label-free detection technique which has been employed for detecting imidacloprid (Homola et al., 1999; Dinga et al., 2012; Ding and Yang, 2013). Commercial sensing platforms utilize an optical prism to induce propagating surface plasmon polaritons in thin noble films and enable real-time and label-free measurements of biomolecular binding affinity. In addition to the prism coupling method, metallic nanostructures offer a simpler way for SPR excitation (Raether, 1988; Ebbesen et al., 1998; Stewart et al., 2008; Anker et al., 2008). Periodic metallic nanohole, nanoslit or nanogrid arrays have been utilized for biosensing applications (Brolo et al., 2004; Gordon et al., 2008; Im et al., 2011; Brolo, 2012; Lee et al., 2007, 2012a, 2012b). However, the majority of SPR sensing is performed on dedicated and expensive instruments. In this study, we combined an indirect competitive immunoassay, capped-nanoslit-based SPR biochip and simple portable imaging system for label-free detection of imidacloprid pesticides. The sensing chip, similar to a tiny spectral analyzer, consists of several capped nanoslit arrays with different periods. The distribution of the transmitted light from these arrays comprises a spectral image on the chip. The detection system is a smartphone with a cheap light-emitting diode (LED) and a narrowband filter. When the analyte is on the surface of the chip, the brightest spot of the spectral image is shifted. The qualitative and semiquantitative analyses of the analyte can be conducted by observing the spot shift on the chip through naked eyes or smartphones. We demonstrated simultaneous detection of different concentrations of imidacloprid pesticides. The visual detection limit is about 1 ppb, which is below the maximum residue concentration permitted by law (20 ppb). The lowest detectable concentration for the imidacloprid pesticide can be further improved by using image processing in the smartphone. Such a portable sensing platform takes advantages of multiple detection, semiquantitative and qualitative analyses, rapid determinations, user-friendliness and low cost. It can be utilized for on-site screening of pesticides and considered as a cost-effective complement technique to the chromatography methods.

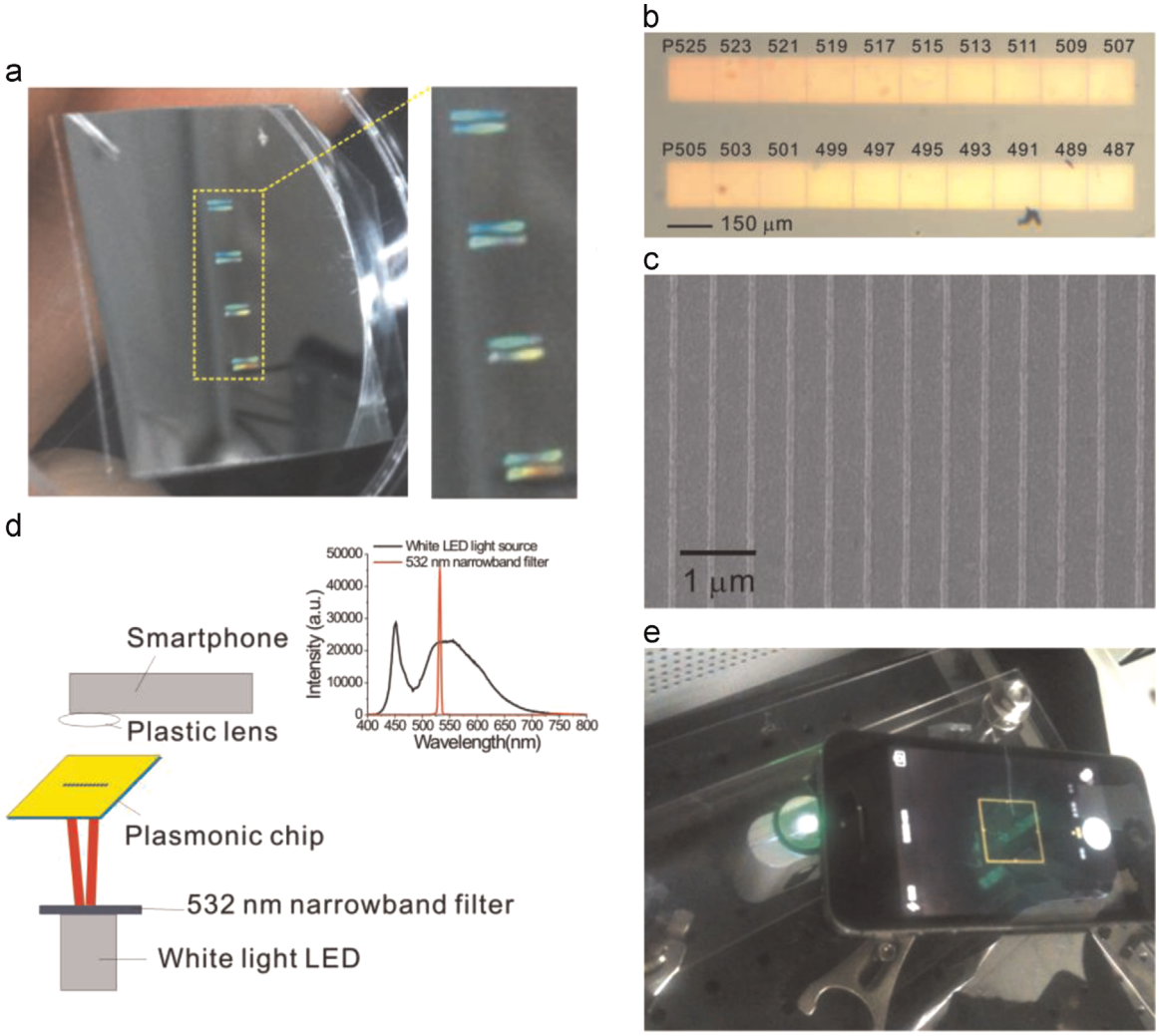

Fig. 1. Fabrication of plasmonic biochips and optical setup. (a) Optical image of the plasmonic biochip. There were four sets of capped nanoslit arrays on the chip. (b) The transmitted light image of the biochip using white light. The period of the nanostructure ranged from 487 to 525 nm. (c) The scanning electron microscope image of a capped nanoslit array with 516 nm period. (d) Schematic configuration of the portable optical system for the image measurement. The system composed of a smartphone, LED light source and narrowband filter. (e) Optical image of the detection system using a smartphone.

2. Material and methods

2.1. Fabrication of plasmonic biochips

The biochip was made on a cyclic olefin polymer (COP) substrate using hot embossing nanoimprint lithography (see Fig. S1). In this study, we fabricated capped nanoslit arrays with different periods ranged from 471 to 525 nm with a step of 2 nm or 3 nm. The area of each nanoslit array was $150 \times 150\ \mu m^2$. Fig. 1(a) shows the optical image of the fabricated biochip. There were four sets of capped nanoslit arrays on the chip. The structure parameters of the four sets of capped nanoslit arrays were the same. The transmitted light image of the biochip using white light is shown in Fig. 1(b). The periods ranged from 487 to 525 nm. The period difference was 2 nm. Fig. 1(c) shows a scanning electron microscope (SEM) image of the nanostructure with a period of 516 nm. The slit width was 80 nm.

2.2. Optical setup

Fig. 1(d) and (e) shows the schematic configuration and optical image of the portable spectral imaging system, which is composed of a smartphone, a commercially available plastic lens, a white LED light source and a narrowband filter. A narrowband green light from the white light and narrowband filter (see Fig. 1(d) inset) was normally incident on the chip. The transmitted light was then collected by a plastic lens and imaged by the charge-coupled device (CCD) in the smartphone. There was no need for image scanning and sample alignment. The smartphone directly recorded the transmission image of the chip. Compared to the prism-based surface plasmon resonance sensing platform, the optical setup is simple and inexpensive.

2.3. Preparation of imidacloprid, protein–hapten conjugates and monoclonal antibodies

Reference standards of imidacloprid (%) were provided by the Agricultural Chemicals and Toxic Substances Research Institute, Taiwan. The imidacloprid was solved in acetone (100 ppm) and then diluted with a 4-(2-hydroxyethyl)-1-piperazineethanesulfonic acid (HEPES) buffer solution. The imidacloprid haptens (1-[(6-Carboxylethylthio-3-pyridinyl)methyl]-N-nitro-2-imidazolidinimine) with 37% (w/w, by GC–MS classification) were synthesized as described (Li and Li, 2000). The procedures for generating the immune response in mice and hybridoma production were similar to those described by Kim et al. (2004). These procedures were generated by GenScript (GenScript, Piscataway, NJ). The details were described in the Supplementary information.

2.4. Immunoassay format and immobilization procedure

As the imidacloprid has a low molecular weight, we employed an indirect competitive immunoassay to enhance the sensitivity and specificity. The chip surface was first immobilized with 100 μg/ml imidacloprid conjugated with bovine serum albumin proteins (imidacloprid–BSA). Then it was exposed to a mixture of imidacloprid and monoclonal anti-imidacloprid antibodies. The imidacloprid in solution competed with imidacloprid–BSA on chip surface for binding the anti-imidacloprid antibodies. In our experiments, imidacloprid samples with different concentrations were mixed with 700 μg/ml anti-imidacloprid antibodies for the indirect competitive immunoassay.

The plasmonic biochip was encapsulated with a 4-nm-thick Al_2O_3 film to protect the Ag film from oxidation. The Al_2O_3 film was coated using an atomic layer deposition (ALD) method. The chip was exposed to a 95% ethanol at room temperature for 5 min to clean the chip surface and purged dry by nitrogen gas. In order to immobilize imidacloprid–BSA on the structure surface, the biochips with a 4-nm-thick Al_2O_3 shell was exposed to a 10% aminopropyltriethoxysilane (APTES) solution for 30 min, washed with 95% ethanol, purged dry by nitrogen gas and then baked at 120 °C for 1 h to form amino groups on the Al_2O_3 film surface. After modification of the amino groups, the surface was activated for amide binding by dipping the chip into a 1 mM disuccinimidyl suberate (DSS) amino reactive bifunctional cross-linker at 25 °C for 30 min. The chip was washed with a dimethylformamide (DMF) solution to remove the unbound cross-linker and purged dry. A 2.5 μL imidacloprid–BSA solution was dropped on the chip at 25 °C for 1 h. After the chip was washed by ultrapure water and purged dry, the imidacloprid–BSA conjugate was covalently bound to the surface. In order to block any free active sites available on the surface, a 20 μL of 1 mg/mL BSA proteins was dropped on the chip. After the unbound BSA proteins were removed by ultrapure water, the chip was ready for the following competitive immunoassay.

In the measurement of imidacloprid, a 0.7 μL monoclonal anti-imidacloprid antibody solution was mixed with a 0.7 μL imidacloprid sample. Competition between free imidacloprid and surface-bound imidacloprid–BSA was begun when the mixture was dropped on the chip. After 20 min of immunoreaction, the chip was washed with a HEPES buffer solution and purged dry. The mixing, dropping, washing and nitrogen-purged dry processes were subsequently repeated for various concentrations of imidacloprid solutions from 10 ppm to 0 ppb.

3. Results and discussion

3.1. Optical characterization of plasmonic chips

Fig. 2(a) shows the measured transmission spectra of the plasmonic biochip in air for normally-incident polarized light. The period ranged from 487 to 525 nm. The period difference between adjacent nanoslit arrays was about 2 nm. The polarization of the incident light was perpendicular to the nanoslits because the gap plasmons in nanoslits and surface plasmons on the periodic surface can only be excited by using transverse magnetic (TM)-polarized incident light (Wei et al., 2002). There are two resonant modes in the capped nanoslit arrays. One is the gap plasmon resonance (cavity mode) in the slit gaps and the other is Bloch wave surface plasmon polariton (BW-SPP) on the periodic silver surface. The cavity mode generates a broadband resonance in the transmission spectrum. The resonant condition is estimated by the Fabry–Perot cavity (Gordon, 2006)

$$2n_{eff}k_0h + \phi_1 + \phi_2 = 2m\pi \tag{1}$$

where n_{eff} is the equivalent refractive index in the slit, k_0 is the free space wavelength vector ($2\pi/\lambda_0$), h is the height of the periodic ridge, and ϕ_1 and ϕ_2 are the phase shifts at the top and bottom interfaces. The resonant wavelength is affected by the slit width and height. In the design of nanoslit array, the resonant wavelength of the cavity mode is around 570 nm. On the other hand, the BW-SPP occurs on the periodic metallic surface when the Bragg condition is satisfied. It generates a narrowband transmission in the measured spectrum. For normally incident light, the Bragg condition for a 1-D array can be described by (Raether, 1988)

$$\lambda_{SPR}(n, i) = \frac{P}{i} Re\{(\frac{\varepsilon_m n^2}{\varepsilon_m + n^2})^{1/2}\} \tag{2}$$

where i is the resonant order, P is the period of the nanostructure, ε_m is the dielectric constant of the metal and n is the environmental refractive index. The resonant wavelength of the BW-SPP is

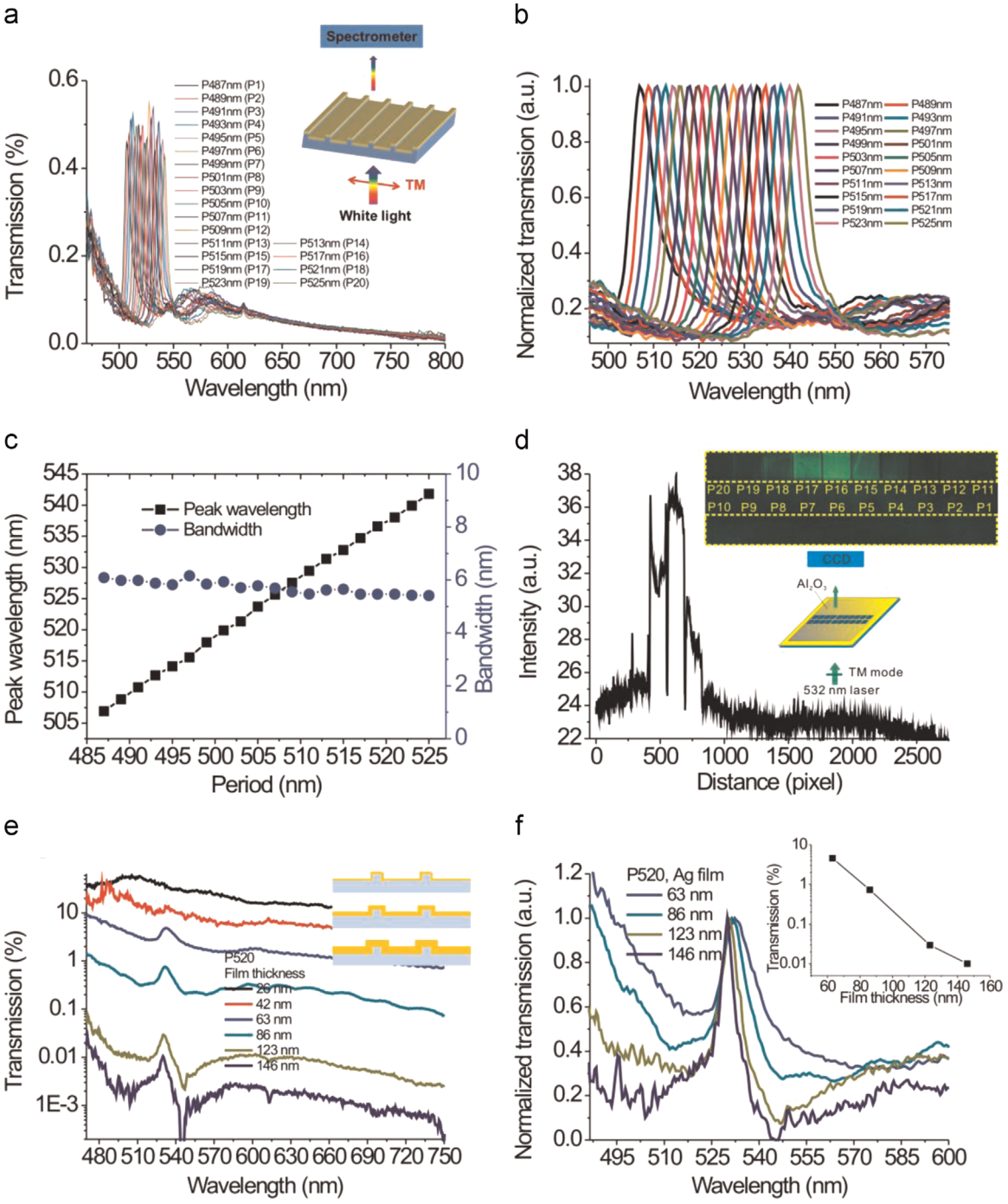

Fig. 2. Optical characterization of plasmonic chips. (a) The measured transmission spectra of the capped silver nanoslits with different period in air for normally-incident TM-polarized light. The periods were from 487 to 525 nm. The period difference was 2 nm. (b) Normalized transmission spectra of the capped metallic nanoslits with different periods. (c) Experimental peak wavelengths of SPR resonances and FWHM bandwidths as a function of period. There was a linear correlation between the peak wavelength and period. The bandwidth ranged from 5.4 to 6.1 nm. (d) The intensity distribution of the transmitted light image indicated with dashed line in the inset. The inset shows the transmitted light image (spectral image) of the biochip using 532-nm laser light. (e) The measured transmission spectra of 520-nm-period capped silver nanoslits with different film thicknesses. (f) Normalized spectra of 520-nm-period capped nanoslits with different film thicknesses. The inset shows the peak transmission as a function of the film thickness. The transmission decreased with the increase of silver film thickness.

in proportional to the period. We designed the periods for generating λ_{SPR} around 530 nm. It is noted that the cavity mode had an overlap with the BW-SPP mode. The coupling of the broadband cavity mode to the narrowband BW-SPP mode generates an asymmetric Fano resonance (Miroshnichenko et al., 2010; Luk'yanchuk et al., 2010). The Fano resonant wavelength occurs near the λ_{SPR}. The capped nanoslit array has a metallic cap on the top of nanoslits. It can efficiently enhance the cavity mode and increases the Fano coupling efficiency as compared to conventional nanoslit array (Lee et al., 2015). Such enhanced Fano mode increased the resonant quality of the surface plasmon resonance. Fig. 2(b) shows the normalized transmission spectra of the capped silver nanoslits with different periods. The measured Fano resonant wavelengths were proportional to the periods and the full width at half-maximum (FWHM) bandwidth of the enhanced Fano resonance was about 5–6 nm (see Fig. 2(c)). Fig. 2(d) inset shows the transmitted light image of the biochip using 532-nm light source. The distribution of the transmitted light through these arrays with

adjacent periods formed a spectral image on the chip as shown in Fig. 2(d). The *x*-axis was related to different period and the *y*-axis was the transmission intensity. It was noted that the thickness of the metallic layer has an important effect on the bandwidth. Fig. 2 (e) shows the measured transmission spectra of 520-nm-period capped silver nanoslits with different thicknesses of silver film from 26 to 146 nm. The bandwidth of the Fano resonance decreased with the increase of the film thickness (see Fig. 2(f)). In the nanoslits, there is no cut-off for the TM-polarized wave. The TM wave can propagate along the slit gaps. The quality of the gap resonance is related to the amplitude of reflection at the upper/lower interface of the slit (Gordon, 2006). The increased film thickness results in a better vertical confinement of the cavity mode. In addition, it provided an enhanced confinement for BW-SPP mode. The coupling of the cavity mode to the BW-SPP mode generated a narrower Fano resonance. Therefore, there is a substantially decrease of the bandwidth of the Fano resonance as the film thickness increases. The narrow resonant bandwidth is important for the direct visualization and a lower limit of detection. It was noted that the transmission of the Fano resonance decreased dramatically with the increase of the film thickness as shown in the inset of Fig. 2(f). The peak transmission decreased about two orders of magnitude when the film thickness increased from 80 to 146 nm (see Fig. 2(f) inset). The low transmittance will result in a large noise in the measurement. In our chips, 80-nm-thick silver film was used for the tradeoff between the bandwidth and the transmission.

3.2. Insecticide detection experiment

We used indirect competitive immunoassay tests for label-free detection of imidacloprid pesticides as shown in Fig. 3(a). Fig. 3

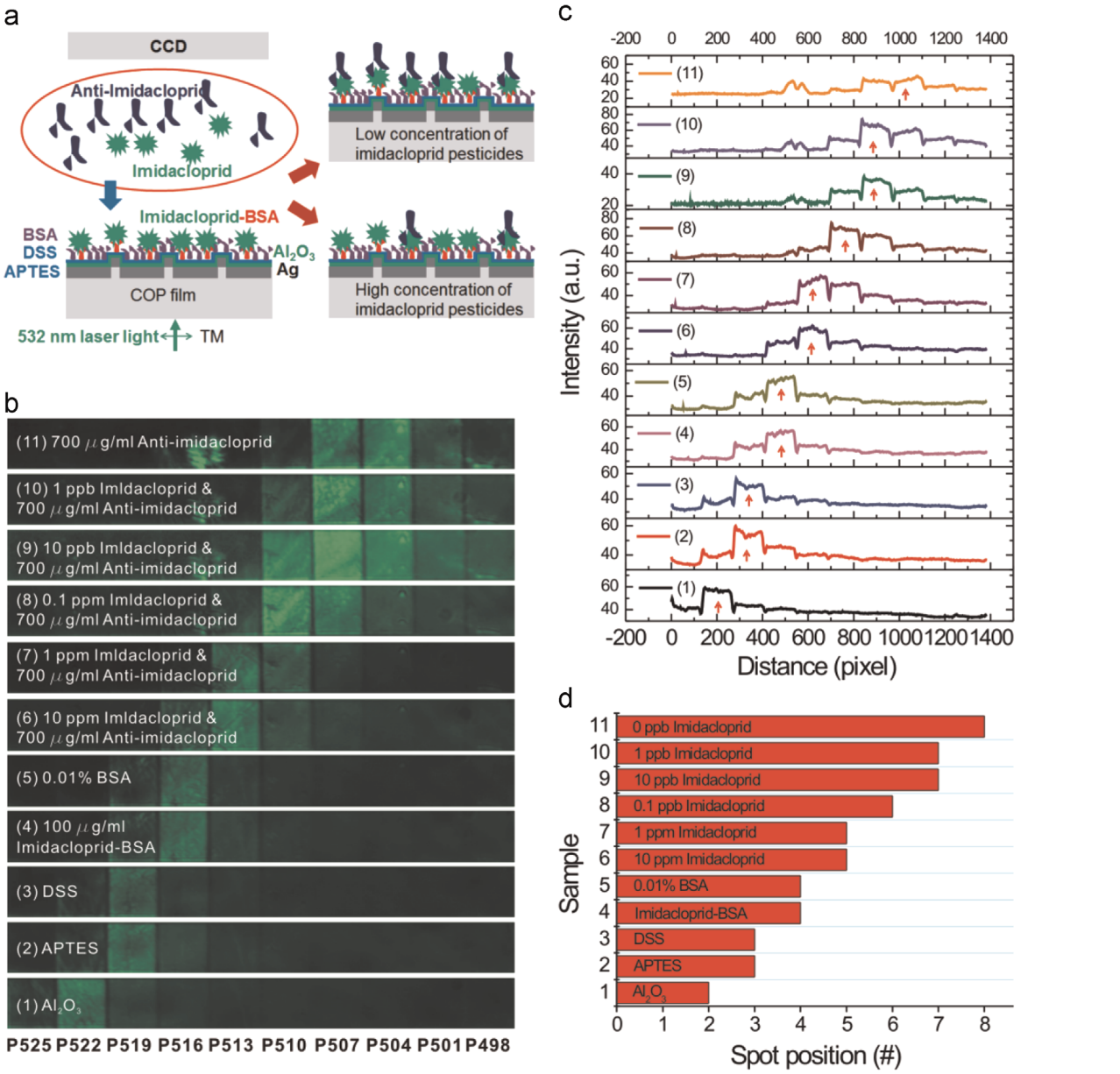

Fig. 3. An indirect competitive immunoassay for label-free detection of imidacloprid pesticides using plasmonic chips. (a) Schematic representation of a competitive immunoassay for label-free detection of imidacloprid pesticides. Low concentration (upper right) and high concentration (lower right) of imidacloprid pesticides. (b) The spectral images of the chip for different surface conditions. The chosen period of the capped nanostructure ranged from 498 to 525 nm. The period difference was 3 nm. (c) The intensity distributions of the spectral images in panel (b) for different surface conditions. (d) The position of the brightest zone of the spectral image against the surface condition. The brightest spot shifted to right with the decrease of the concentration of the imidacloprid pesticide.

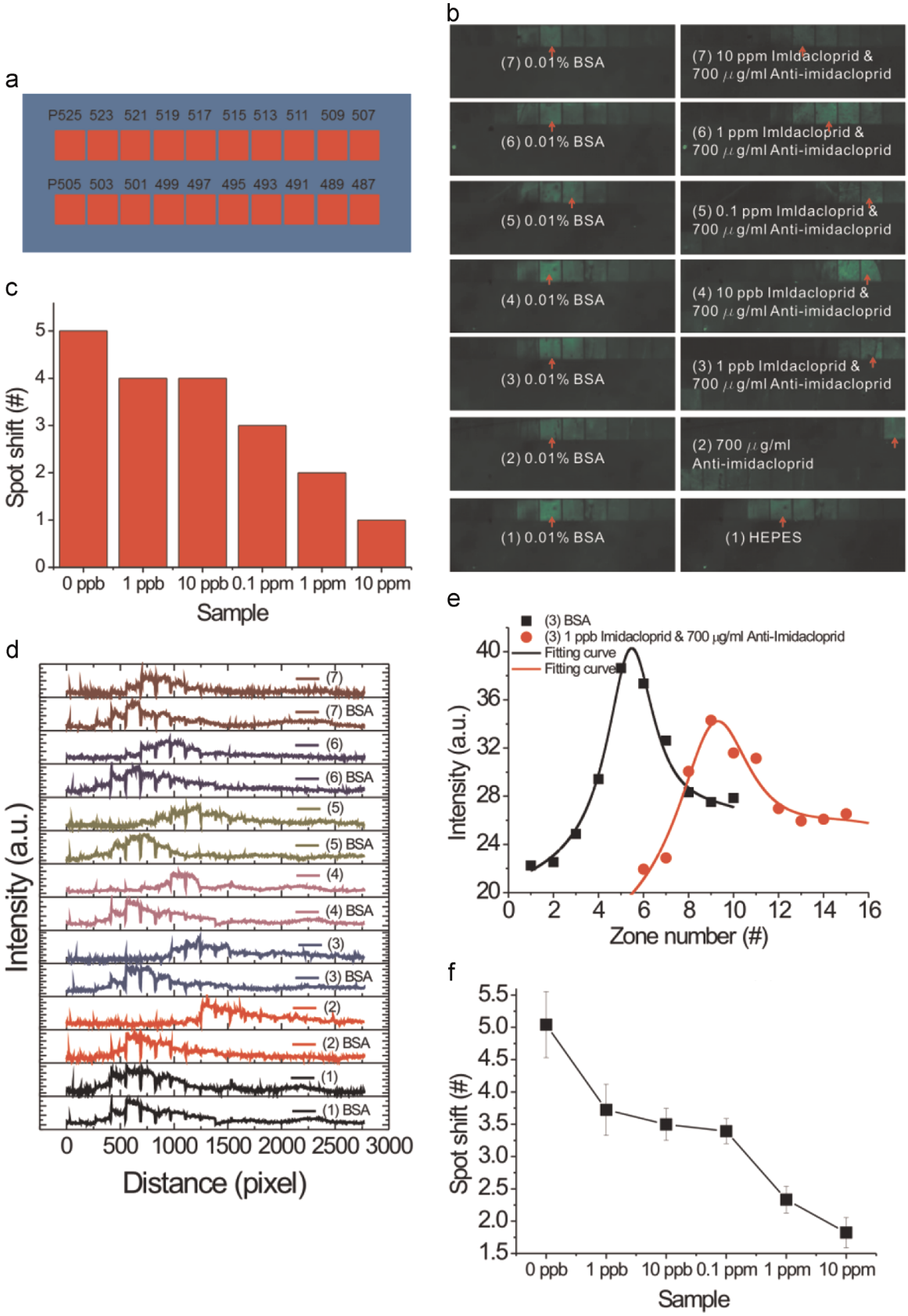

Fig. 4. An indirect competitive immunoassay for label-free detection of imidacloprid pesticides using higher resolution plasmonic chips and the imaging system. (a) The layout of the nanostructures on the chip. The chip was consisted of capped nanoslit arrays with periods ranged from 487 to 525 nm. The period difference was 2 nm. (b) The spectral images of the chip for different surface conditions. (c) The position of the brightest zone of the spectral image against the surface condition. The brightest spot shifted to right with the decrease of the concentration of the imidacloprid pesticide. The detectable concentration of the imidacloprid pesticide was about 1 ppb. (d) The intensity distributions of the spectral images for different concentrations of imidacloprid as shown in panel (b). (e) The intensity distributions of the spectral images and the fitting curves for 0.01% BSA sample and 1 ppb imidacloprid pesticides. The distribution was fitted by a two-peak Lorentz function. (f) The peak shift as a function of the concentration of imidacloprid pesticides using image processing.

(b) shows the spectral images of the chip for different surface conditions. Fig. 3(c) shows the intensity distributions of the spectral images in Fig. 3(b) for different surface conditions. At first, the brightest zone located at 522-nm-period nanostructure (Zone 2) when the biochip was encapsulated with a 4-nm-thick Al_2O_3 shell. After the modification of amino groups using APTES, the brightest zone moved to 519-nm-period nanostructure (Zone 3). The brightest zone was still at 519-nm-period nanostructure (Zone 3) when the DSS bifunctional cross-linker was bound to the surface. Next, when the imidacloprid–BSA conjugate was covalently bound to the structure surface, the brightest zone shifted 1 block (Zone 4). The position of the brightest zone remained unchanged (Zone 4) after the BSA coating process. After detecting the monoclonal anti-imidacloprid–BSA antibody and 10 ppm imidacloprid mixture, we found that the brightest zone shifted 1 block (Zone 5). The brightest zone moved from Zone 5 to Zone 8 when the concentration of the imidacloprid solution was decreased from 10 ppm to 0 ppb as shown in Fig. 3(d). It is noted that intensity distribution was sharp for the Al_2O_3 coated biochip. As the increase of surface binding molecules, the intensity distribution was broadened as seen in Fig. 3(b). It was attributed to the non-uniform immobilization of probes and adsorption of the analytes on the chip surface. Such non-uniform molecular layer destroyed the resonance of BW-SPP mode.

To compare the results with conventional measurements using a spectrometer, we also measured transmission spectra of the capped nanoslit arrays (see Fig. S4). The peak wavelength shifts from the transmission spectra match quite well with the brightest zone shifts in the spectral images. In Fig. S4, the noise level on the measurement at 0 ppm was 9.7%. Therefore, the lowest detectable concentration for the imidacloprid pesticide was about 0.2 ppb (0.2 ng/mL) using the spectral measurement. We further compared the results with previous techniques. For the indirect competitive strip assay, the strip has a visual detection limit for imidacloprid at 0.5 ng/mL and allows distinguishing the imidacloprid semiquantitatively in three concentration intervals: <0.5 ng/mL, 0.5–2 ng/mL, and >42 ng/mL (Xu et al., 2012). On the other hand, the limits of detection (LODs) of imidacloprid for an indirect competitive ELISA (icELISA) method is 0.08 ng/mL and the working range is 0.1–4.0 ng/mL (Kim et al., 2004). Therefore, compared to those label detection techniques, the proposed label-free biochip has a comparable sensitivity but wider working range. Such a sensitive chip could allow the detection of the imidacloprid pesticide below the maximum residue concentration permitted by law (0.01 mg/kg, 10 ppb). It was noted that the sensitivity of the chip can be further increased by reducing the bandwidth and decreasing the period difference (or the spectral resolution) to 1 nm. The bandwidth can be narrowed by increasing the silver film thickness and decreasing the slit width (Lee et al., 2015). However, it results in a low transmission. A high-power and stable light source is required for the measurement. In addition, the spectral images can be analyzed with a spectral integration method, which can increase the signal-to-noise ratio of the system and effectively improve the sensing capability (Stewart et al., 2006).

3.3. *A simple portable spectral imaging system for detecting imidacloprid pesticides*

In order to fulfill the requirement of on-site diagnostics, we further developed a simple, inexpensive and portable imaging system and applied it to qualitatively and semiquantitatively detect imidacloprid pesticides. Fig. 4(a) shows the layout of the capped nanoslit arrays on the chip. The chip was consisted of nanoslit arrays with periods ranged from 487 to 525 nm. The period difference was 2 nm. Fig. 4(b) shows the images of the chip for detecting six different concentrations of imidacloprid pesticides using a smartphone (Iphone 4S). Obviously, the position of the brightest spot remains unchanged for the detection of the HEPES buffer solution. The images difference between 0 ppb and 1 ppb imidacloprid samples can be easily distinguished through naked eyes. Fig. 4(c) shows the shift of bright spot with respect to the HEPES buffer condition. The brightest zone moved 5, 4 and 1 block for 0 ppb, 1 ppb and 10 ppm imidacloprid solutions, respectively. The images difference between 0 ppb and 1 ppb imidacloprid samples can be easily distinguished through CCD image. There was an inverse correlation between the brightest block shift and the concentration of the imidacloprid pesticide. As the immunobinding of anti-imidacloprid antibodies on the chip surface will be inhibited by imidacloprid present in solution and thus the block shift will decrease with increasing concentrations of imidacloprid.

As the naked eye can only judge period difference between adjacent arrays, it is difficult to distinguish between both solutions due to the limited resolution (2 nm/Block). For example, the 1 ppb and 10 ppb show the same spot shift in Fig. 4(c). Nevertheless, the spectral image difference between both samples can be distinguished using image processing. Fig. 4(d) shows the intensity distributions of the spectral images for different concentrations of imidacloprid. Even the brightest spot located at the same area, the intensity distribution versus the period is different. The distribution can be fitted with resonant functions to refine the position of peak value. As an example, Fig. 4(e) shows the intensity distributions of the spectral images and the fitting curves for 0.01% BSA sample and 1 ppb imidacloprid pesticides. The distribution was fitted by a two-peak Lorentz function. The fitting curves show that the peak shift was 3.723 blocks. As compared to direct bright-zone observation, the position shift is 4 blocks. Using the imaging process, more accurate position shift can be found. Fig. 4(f) shows the peak shift as a function of the concentration of imidacloprid pesticides using image processing with the two-peak Lorentz function. The peak shifts for 1 ppb and 10 ppb imidacloprid solutions were well distinguished. Such image processing procedure can be written as a mobile application (APP) software. Therefore, more precisely semiquantitative analyses can be completed by using the smartphone.

4. Conclusions

We demonstrated an easy, low-cost and label-free detection technique for qualitative and semiquantitative analyses of imidacloprid pesticides. No other expensive instruments are required. The concentration levels of the imidacloprid pesticides can be directly estimated through naked eyes. The visual detection limit is about 1 ppb. The precisely semiquantitative analyses of the analyte can be completed by using image processing in smartphones. The detection limit is better than 1 ppb. Compared to the one-step strip assay, the proposed chip is capable of semiquantitative analyses and multiple detection. (see Fig. S2). Compared to the enzyme-linked immunosorbent assay, our method is label-free and requires simple washing steps and short reaction time. In addition, the label-free chip has a comparable sensitivity but wider working range than those labeling techniques. Such a portable sensing platform possesses several advantages, including multiple detection, semiquantitative and qualitative analyses, rapid determinations, user-friendliness and low cost. It can be utilized for on-site screening of pesticides and considered as a cost-effective complement technique to the chromatography methods. For specificity tests, the monoclonal antibodies play a key role. We have tested the specificity of monoclonal anti-imidacloprid antibodies to the imidacloprid, thiamethoxam and dinotefuran pesticides by the

icELISA method. It confirms that monoclonal antibodies used in the experiments were specific for the imidacloprid pesticides (see Fig. S3). In our future work, the number of sensing zones will be further increased, various antibodies will be produced and multiple pesticides will be detected simultaneously using the chips.

Acknowledgments

This work was supported by Ministry of Science and Technology, Taipei, Taiwan, under Contract no. MOST 103-2221-E-001-013-MY3 and by the Bureau of Animal and Plant Health Inspection and Quarantine of Taiwan, under Contract no. 103AS-14.2.3-BQ-B1. Technical support from the core facilities for nanoscience and nanotechnology and the scientific instrument facility at Institute of Chemistry, Academia Sinica in Taiwan, is acknowledged.

Appendix A. Supplementary material

Supplementary data associated with this article can be found in the online version at http://dx.doi.org/10.1016/j.bios.2015.08.010.

References

Anker, J.N., Hall, W.P., Lyandres, O., Shah, N.C., Zhao, J., Van Duyne, R.P., 2008. Nat. Mater. 7, 442–453.
Brolo, A.G., Gordon, R., Leathem, B., Kavanagh, K.L., 2004. Langmuir 20, 4813–4815.
Brolo., A.G., 2012. Nat. Photonics 6, 709–713.
Ding, X., Yang, K.L., 2013. Anal. Chem. 85, 5727–5733.
Ding, X., Zhang, W., Cheng, D., He, J., Yang, K.L., 2012. Biosens. Bioelectron. 35, 271–276.
Ebbesen, T.W., Lezec, H.J., Ghaemi, H.F., Thio, T., Wolff, P.A., 1998. Nature 391, 667–669.
Fang, S., Zhang, B., Ren, K.W., Cao, M.M., Shi, H.Y., Wang, M.H., 2011. J. Agric. Food Chem. 59, 1594–1597.
Gordon, R., 2006. Phys. Rev. B 73, 153405.
Gordon, R., Sinton, D., Kavanagh, K.L., Brolo, A.G., 2008. Acc. Chem. Res. 41, 1049–1057.
Goulson, D., 2013. J. Appl. Ecol. 50, 977–987.
Hallmann, C.A., Foppen, R.P.B., van Turnhout, C.A.M., de Kroon, H., Jongejans, E., 2014. Nature 511, 341–343.
Henry, M., Beguin, M., Requier, F., Rollin, O., Odoux, J.F., Aupinel, P., Aptel, J., Tchamitchian, S., Decourtye, A., 2012. Science 336, 348–350.
Homola, J., Yee, S.S., Gauglitz, G., 1999. Sens. Actuator B: Chem. 54, 3–15.
Im, H., Lee, S.H., Wittenberg, N.J., Johnson, T.W., Lindquist, N.C., Nagpal, P., Norris, D. J., Oh, S.H., 2011. ACS Nano 5, 6244–6253.
Kim, H.J., Shelver, W.L., Li, Q.X., 2004. Anal. Chim. Acta 509, 111–118.
Kim, H.J., Shelver, W.L., Hwang, E.C., Xu, T., Li, Q.X., 2006. Anal. Chim. Acta 571, 66–73.
Lee, K.L., Lee, C.W., Wang, W.S., Wei, P.K., 2007. J. Biomed. Opt. 12, 044023.
Lee, K.L., Huang, J.B., Chang, J.W., Wu, S.H., Wei, P.K., 2015. Sci. Rep. 5, 8547.
Lee, K.L., Chen, P.W., Wu, S.H., Huang, J.B., Yang, S.Y., Wei, P.K., 2012. ACS Nano 6, 2931–2939.
Lee, K.L., Chih, M.J., Shi, X., Ueno, K., Misawa, H., Wei, P.K., 2012. Adv. Mater. 24, OP253–OP259.
Li, K., Li, Q.X., 2000. J. Agric. Food Chem. 48, 3378–3382.
Luk'yanchuk, B., Zheludev, N.I., Maier, S.A., Halas, N.J., Nordlander, P., Giessen, H., Chong, C.T., 2010. Nat. Mater. 9, 707–715.
Miroshnichenko, A.E., Flach, S., Kivshar, Y.S., 2010. Rev. Mod. Phys. 82, 2257–2298.
Posthuma-Trumpie, G.A., Korf, J., van Amerongen, A., 2009. Anal. Bioanal. Chem. 393, 569–582.
Raether, H., 1988. Surface Plasmons on Smooth and Rough Surfaces and on Gratings. Springer-Verlag, Berlin.
Stewart, M.E., Anderton, C.R., Thompson, L.B., Maria, J., Gray, S.K., Rogers, J.A., Nuzzo, R.G., 2008. Chem. Rev. 108, 494–521.
Stewart, M.E., Mack, N.H., Malyarchuk, V., Soares, J.A.N.T., Lee, T.W., Gary, S.K., Nuzzo, R.G., Rogers, J.A., 2006. Proc. Natl. Acad. Sci. USA 103, 17143.
Van der Sluijs, J.P., Amaral-Rogers, V., Belzunces, L.P., Bijleveld van Lexmond, M.F.I.J., Bonmatin, J.M., Chagnon, M., Downs, C.A., Furlan, L., Gibbons, D.W., Giorio, C., Girolami, V., Goulson, D., Kreutzweiser, D.P., Krupke, C., Liess, M., Long, E., McField, M., Mineau, P., Mitchell, E.A.D., Morrissey, C.A., Noome, D.A., Pisa, L., Settele, J., Simon-Delso, N., Stark, J.D., Tapparo, A., Van Dyck, H., van Praagh, J., Whitehorn, P.R., Wiemers, M., 2015. Environ. Sci. Pollut. Res. 22, 148–154.
Wang, R., Wang, Z., Yang, H., Wang, Y., Deng, A., 2012. J. Sci. Food Agric. 92, 1253–1260.
Watanabe, E., Miyake, S., Yogo., Y., 2013. J. Agric. Food Chem. 61, 12459–12472.
Watanabe, E., Eun, H., Baba, K., Arao, T., Ishii, Y., Endo, S., Ueji, M., 2004. Anal. Chim. Acta 521, 45–51.
Wei, P.K., Chou, H.L., Fann, W.S., 2002. Opt. Express 10, 1418–1424.
Whitehorn, P.R., O'Connor, S., Wackers, F.L., Goulson, D., 2012. Science 336, 351–352.
Xu, T., Xu, Q.G., Li, H., Wang, J., Li, Q.X., Shelver, W.L., Li, J., 2012. Talanta 101, 85–90.